Spatial Phase Synchronisation of Pistachio Alternate Bearing

Kenshi Sakai (ken@cc.tuat.ac.jp)
Tokyo University of Agriculture and Technology
Patrick Brown
UC Davis https://orcid.org/0000-0001-6857-8608
Todd Rosenstock
Center for International Forestry Research-World Agroforestry https://orcid.org/0000-0002-1958-9500
Shrinivasa Upadhyaya
University of California, Davis
Alan Hastings
University of California

Article

Keywords: nonlinear physics, agroecosystems, pistachio trees

Posted Date: September 8th, 2021

DOI: https://doi.org/10.21203/rs.3.rs-877774/v1

Spatial Phase Synchronisation of Pistachio Alternate Bearing

Kenshi Sakai[1], Patrick Brown[2], Todd Rosenstock[3], Shrini Upadhyaya[4], Alan Hastings[5,6]

[1]Department of Environmental and Agricultural Engineering, Tokyo University of Agriculture and Technology, Fuchu, Tokyo 183-8509, Japan.

[2]Department of Plant Science, University of California, Davis, CA 95616, USA.

[3] Department of Land Health Restoration, Consultative Group on International Agricultural Research,

[4]Department of Biological and Agricultural Engineering, University of California, Davis, CA 95616, USA.

[5]Department of Environmental Science & Policy, University of California, Davis, CA 95616, USA.

[6]Santa Fe Institute,1399 Hyde Park Rd., Santa Fe, NM 87501, USA.

Abstract

Nonlinear physics and agroecosystems can be of great relevance in the synchronisations of chaotic oscillators. The endogenous dynamics of the seed production of perennial plant species which include alternate bearing and masting, portray typical synchronisation patterns in nature and can be modelled using a tent map known as a resource budget model (RBM). This study investigates the collective rhythm in 9,562 pistachio trees caused by their endogenous network dynamics and exogenous forces (common noise). Common noise and a local coupling of RBMs are the two primary factors emerging from the bearing phase synchronisation in this orchard. The in-phase/out-of-phase analysis technique quantifying the strength of the phase

synchronisation in trees (population /individual) allows us to study the observed spatial synchrony in detail. We demonstrate how three essential factors, i.e. (a) common noise, (b) local direct coupling, and (c) the gradient of the cropping coefficient, explain the spatial synchrony of the orchard. Here, we also show that the methodology employing nonlinear physics to study agroecological systems can be useful for resolving practical problems in agriculture including yield variability and spatial synchrony which often compromise efficient resource management.

INTRODUCTION

Alternate bearing (biennial bearing) is a common synchronisation in several tree crops in which a year of heavy yield (on-year state) is followed by a light yield (off-year state). Citrus (e.g. oranges, lemons, and mandarins) and nuts (e.g. pistachio, pecan, and walnuts) are typical alternate bearing crops [1-9] that generally show dominant period-two cycle synchronisation. Masting is also a prevalent synchronisation among tree species in which there are multiple and mixed cycles (i.e. period-two, period-three, period-four, or a combination of them)[10-14]. Such a large on-off period-two cycle of crop production negatively affects profitability and resource (water, nutrient, labor) efficiency. To obtain the knowledge to suppress or predict alternate bearing, the strength of the spatial synchrony should be measured in both individual trees and a population. As the conventional index of synchronisation $SYNC = \frac{S_{by}}{S_{wy}S_{by}}$ (S_{by} : standard deviation of between years, S_{wy} :within years standard deviation) is based on "amplitude" synchronisation, the index determines the degree of synchrony only for a given population[12-14]. Instead, by focusing on "phase" synchronisation, Prasad et al. (2017)

and Sakai et al. (2019) developed an in-phase/out-of-phase analysis technique[15] that enables us to determine the strength of the phase synchrony both in individual and population levels for Citrus and *Zerkova seratta*[16]. The yield data that were analysed here are remarkable since they included measurements pertaining to 9,562 trees obtained over five years[17]. In this study, by introducing the in-phase/out-of-phase analysis technique, we successfully determined the strength of the phase synchronisation in individual trees and uncovered unique and important features of spatial synchrony in the orchard, i.e. (1) a west-east running gradient of the strength of the in-phase synchronisation, and (2) the mode transition between "order" (in-phase synchronisation) and "disorder" over spatial and temporal (year) domains. Additionally, we demonstrated the spatial distribution of the fraction of the period-two cycle for each tree and each year.

A resource budget model (RBM), which is a tent map[18], has been previously used to model the dynamics of seed production of perennial plant species[7-9, 12-17]. For cross-pollinating species, the global coupled map (GCM) and local coupled map (LCM) of RBMs have been used with mean-field pollen coupling to establish the pollen limitation theory as an endogenous mechanism[12-14, 18-20]. Conversely, the pollen limitation theory cannot be observed for deciduous species such as pistachio, as male trees supply pollen to female trees and pollen coupling between female trees never occurs. Instead, the concept of common noise-induced synchronisation (CNIS) was introduced to explain the alternate bearing of pistachio trees[7-9,21]. These models are all prevalent in nonlinear physics[22-26]. Common noise synchronization is a phenomenon in which a nonlinear (even chaotic) oscillator population is synchronized when an irregularly fluctuating external force acts identically on all the oscillators.

A long-range spatial correlation was observed and the presence of local coupling and the direct coupling premising underground root grafting/mycorrhizal networks[1, 27-32] was hypothesised based on the Ising model[17,18,21]. However, the conventional diffusive coupling of RBMs helps enhance the out-of-phase motion (Prasad et al. 2017)[15] because it is implemented to suppress the alternate bearing of Citrus. In this study, while we maintain the hypothesis of the presence of local direct coupling, we implement a novel diffusive coupling that enhances the in-phase synchronisation. For the same purpose, Esmaeili et al. (2020) replaced the RBM with a single-humped map[33-35].

In this study, by applying the in-phase/out-of-phase technique on both the yield data of the orchard and the numerical experiments, we concluded that (a) common noise, (b) local interactions, and (c) the spatial gradient of the cropping coefficient (the control parameter of the RBM) were essential factors that could help explain unique features such as (1) a west-east running gradient of the strength of the in-phase synchronisation, and (2) the mode transition between "order" (in-phase synchronisation) and "disorder" over spatial and temporal (year) domains. Critical discussions on the hypothesis regarding local coupling are presented at the end of the paper. Furthermore, we investigate the importance of nonlinear physics in agroecological systems and farm management.

RESULTS

Spatial phase synchronisation identified in the orchard

Figure 1 shows the spatial phase synchronisation in the orchard.

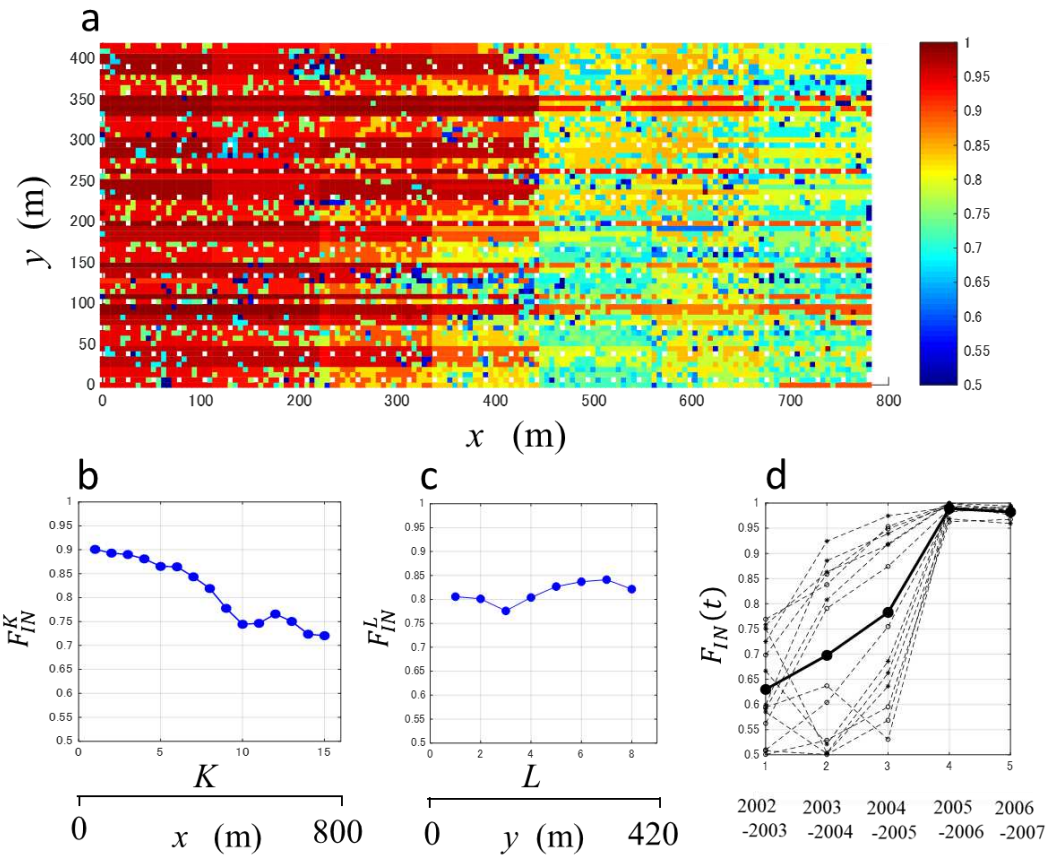

Figure 1. Spatial distributions of the in-phase synchronisation in the orchard.

(a) The actual f_{IN}^i map for 2002–2007 in eight blocks (7 West-East × 2 South-North); (b) Averaged West-East gradient of F_{IN}^k for 2002–2007; (c) Averaged South-North gradient of F_{IN}^L for 2002–2007; (d) time (year) evolution of $F_{IN}(t)$.

To explain the spatial synchrony of the orchard ,the indices for phase synchronisations were defined as described in the Method-Statistics section. Figure 1(a) displays the spatially distributed fraction of the in-phase ($f_{in}^i(t)$) for 9,562 individual trees from 2002–2007. To conduct this analysis the orchard was divided into fourteen blocks by rows and columns: (row, column) = (2 × 7). f_{in}^i were calculated for each tree *i* within the block to which tree *i* belonged to. f_{in}^i was high enough to reach 1.0 in the west blocks and was as low as 0.7 in the east blocks. Figure 1(c) shows F_{IN}^K (K = 1,

2, …, 30), which is the average f_{in}^{i} for every five columns. F_{IN}^{L} (L = 1, 2, …, 9) is the south to north directional average of f_{in}^{i} for every nine rows. F_{IN}^{K} drops from 0.92 to 0.7 from west to east (Fig. 2(b)). Conversely, only a small gradient of F_{IN}^{L} was observed along the south-north direction (Fig. 2(c)). These results indicate that the strength of the phase synchronisation significantly decreases from west to east but is trivial in the south-north direction. In other words, a significant mode transition can be observed from order to disorder in the west-east direction since perfect synchronisation (order) and desynchronization (disorder) of a population corresponds to F_{IN} to 1.0 and 0.5 respectively. In Fig.1(d), the total fraction of in-phase (F_{IN}(t)) increased from 0.62 to 1.0 indicating perfect synchronisation occurred in [2005-2006] and [2006-2007] periods.

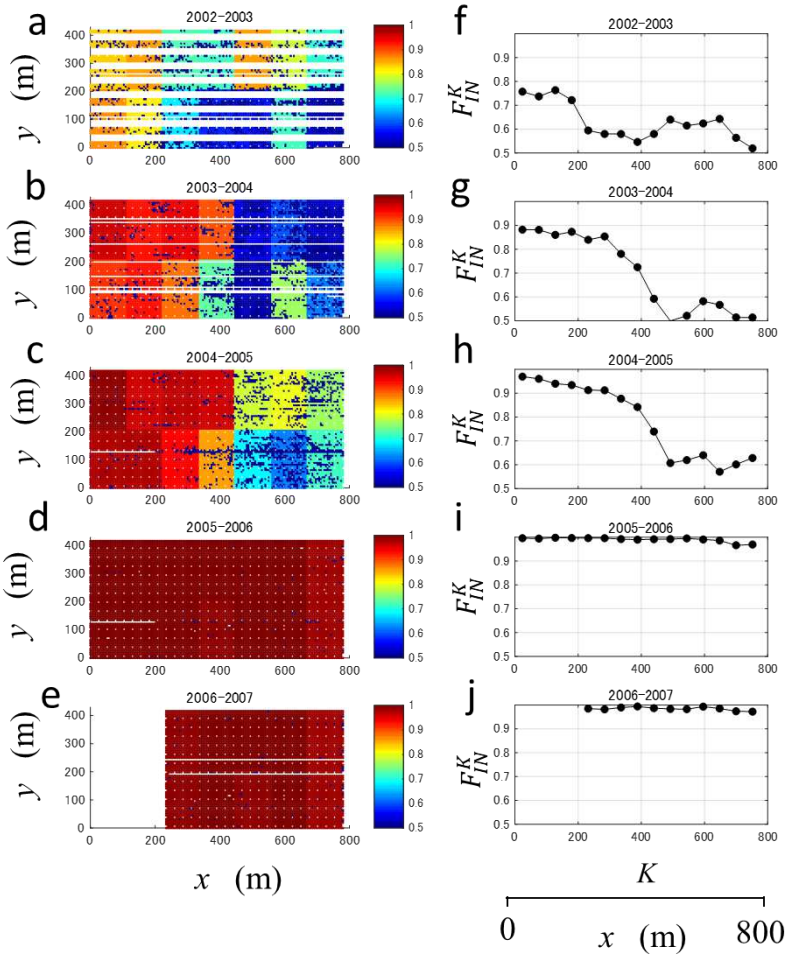

Figure 2. Time evolution of the spatial transition of the phase synchronisation

(a)-(e) The time (year) changes of the spatial phase synchronisation: $f_{IN}^{i}(t)$ maps for 2002–2003, 2003–2004, 2004–2005, 2005–2006 , and 2006–2007 periods in the orchard

(f)-(j) The gradient of the strength of the phase synchronisation: $F_{IN}^{K}(t)$ vs. K plots for 2002–2003, 2003–2004, 2004–2005, 2005–2006 ,and 2006–2007 periods in the orchard

Figure 2 shows the time evolution of the spatial distribution of phase synchronization in the five periods of two successive years: [2002-2003], [2003-2004],[2004-2005],[2005-2006] and [2006-2007] in five rows, respectively. The first and second columns represent the spatial distributions of f_{in}^{i} and $F_{IN}^{K}(t)$ vs. K plot. In the first period

(2003–2004), the strength of phase synchronization and spatial distribution of phase synchronization were weak compared to other periods, which is shown in Fig.2(a) and Fig.2(f).

From the second to the third period, the strength of phase synchronization in the whole orchard increased, and at the same time, the spatial distribution of phase synchronization from west to east became clear, that is, it was stronger in the west and weaker in the east. In fact, $F_{IN}^{1}(2004)$ and $F_{IN}^{30}(2004)$ were 0.98 and 0.56, indicating perfect phase synchronization and desynchronization, respectively.

From the second to the third period;[2003-2004] and [2004-2005], the strength of phase synchronization increased in the whole orchard, and at the same time, the spatial distribution of phase synchronization from west to east became distinct, that is, it was stronger in the west and weaker in the east. In fact, $F_{IN}^{1}(2004)$ and $F_{IN}^{30}(2004)$were 0.98 and 0.56, indicating perfect phase synchronization and desynchronization, respectively. Finally, for the fourth [2005–2006] and fifth [2006–2007] periods, the perfect phase synchronisations dominate over the orchard; thus, $f_{in}^{i}(2006)$ and $f_{in}^{i}(2007)$ reach 1.0 over the entire orchard, and $F_{IN}^{K}(t); (t = 2005\ and\ 2006)$ values are almost always 1.0 for the whole orchard and *K*, indicating that perfect phase synchronisations (i.e. perfect order) occurred from west to east of the orchard. Very importantly, the perfect synchronization mode lasted for two periods [2005-2006] and [2006-2007]. This is clear experimental evidence that mode-locking can occur in a real orchard.

Figures 1 and 2 show that the mode transition between “order” and “disorder” emerge both spatially and temporally (annually) in the orchard. As described above, the index of the fractions of the in-phase such as $f_{in}^{i}(t), f_{in}^{i}, F_{IN}^{K}(t)$ and F_{IN}^{K} successfully describe

detailed information on how the features of phase synchronisations behave both spatially and temporally.

The states of "on-year" and "off-year"

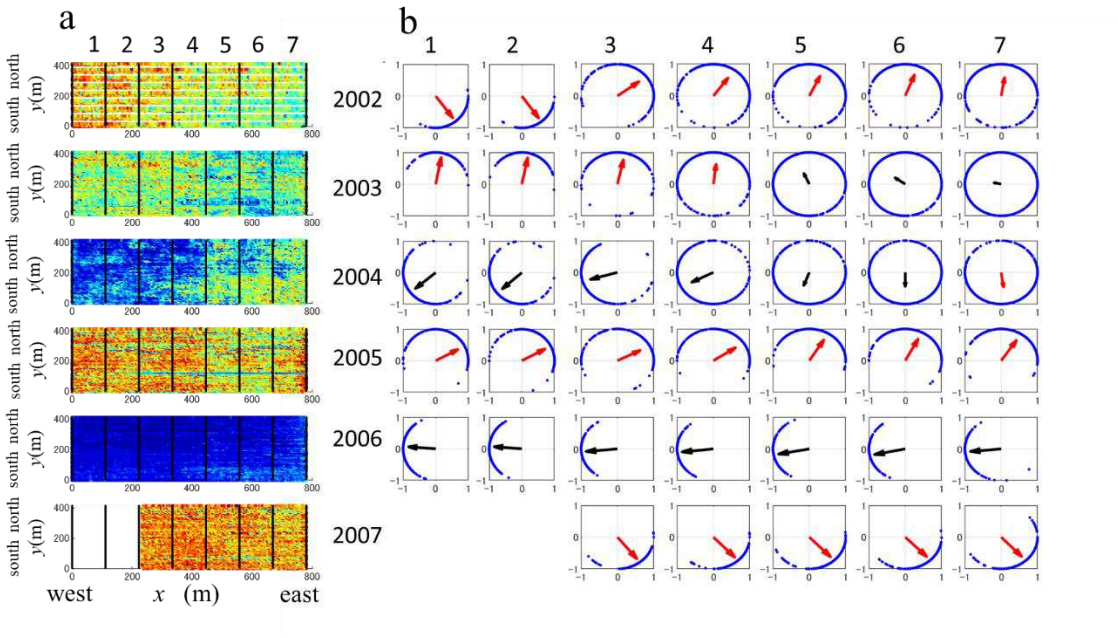

Figure 3 Spatial and annual transitions of the states of "on-year" and "off-year" for individual trees expressed by circle maps.

(a) Yield maps for 2002 through to 2007.

(b) Circle maps for the fourteen blocks for six years (2002–2007). The blue dot mark $(\cos\theta_i, \sin\theta_i)$ on the circumference represents the state of tree *i*. The vectors represent the on-off state of sub-populations of each block and on and off correspond to the red and black ink, respectively.

In this section, we identify the states of the "on-year" and "off-year" of a population by introducing the phase synchronisation analysis technique (see METHODS section). The phase angle $\theta_i(t)$ of each tree for each year calculated from eq.(7) determined the "on" and "off" states for the individual trees. The states of "on-year" and "off-year" are

defined by the period of time covered as follows; an on-year is one in which the phase angle θ is positive, or the yield $x(\mathrm{t})$ is greater than the average yield of the period $\bar{x}(\mathrm{t})$ and vice versa[16].

$$\begin{array}{ll} \text{on}-\text{year:} & \cos\ \theta > 0\ \ or\ \ x(\mathrm{t}) > \bar{x}(\mathrm{t}) \\ \text{off}-\text{year:} & \cos\ \theta \leq 0\ \ or\ \ x(\mathrm{t}) \leq \bar{x}(\mathrm{t}) \end{array} . \quad (1)$$

The vector point for each subpopulation block is given by the mean of all coordinates of the dots i.e. $(\frac{1}{n}\sum_{i=1}^{n}\cos\theta_i(t)\,,\frac{1}{n}\sum_{i=1}^{n}\sin\theta_i\,(t))$, where *n* is the subpopulation size. The amplitude of the vector is the order parameter $p(t)$ of the subpopulation.

$$p(t) = \sqrt{(\frac{1}{n}\sum_{i=1}^{n}\cos\theta_i(t))^2 + (\frac{1}{n}\sum_{i=1}^{n}\sin\theta_i\,(t))^2}. \quad (2)$$

Values $p = 1$ and 0 represent perfect phase synchronisation and desynchronisation, respectively. The "on-year" and "off-year" states of the population are distinguished by the red and black arrows. For example, in 2002 and 2007, all seven blocks are "on-year" states and the states are identical between the seven sub-populations and the whole population. However, in 2003, the state of each subpopulation shifted from a weak "on-year" state to "off-year" states in west to east. The coexistence of the "on-year" and "off-year" states within pistachio orchards has only been known as general qualitative knowledge. With this novel technique, we can quantitatively visualise the coexistence of the "on-year" and "off-year" states of individual trees in both spatial and temporal (annual) domains.

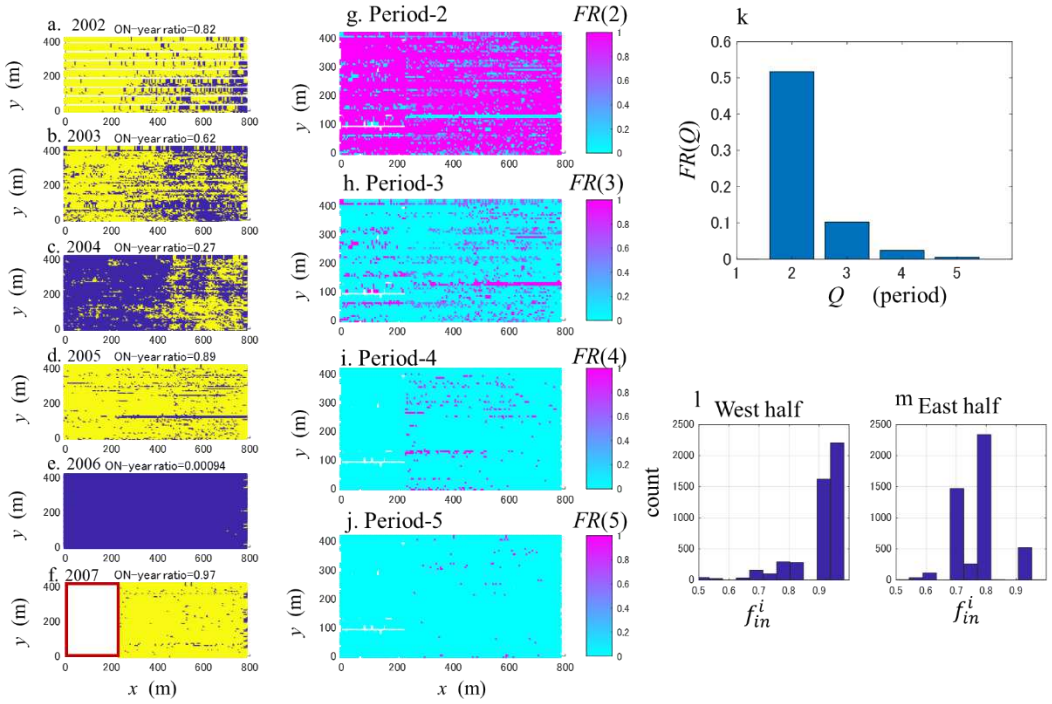

Figure 4 Spatial distribution of the periodic components for individual trees and the compositions of *FR*(Q) in the population.

(a)-(f) On-off states of each trees for six years

(g)-(j) Spatial distribution of individual fraction of period FR_i(Q) for period-two (Q=2), period-three(Q=3), period-four(Q=4) and period-five (Q=5), respectively.

(k) The components of the periodic components *FR*(Q) of the population.

(l) Histogram of $f_{\mathrm{in}}^{\mathrm{i}}$ in the west half of the orchard.

(m) Histogram of $f_{\mathrm{in}}^{\mathrm{i}}$ in the east half of the orchard

Figure 4 shows the composition of periods in individual trees and the population. Several researchers have reported that alternate bearing of pistachios do not always exhibit a clear two-year cycle but may feature various types of synchronisations both spatially and annually[20,36-38]. Sakai et al. (2019) proposed a practical approach to determine the composition of periodic components of alternate bearing and masting of plant populations[16]. For instance, period-two and period-three sequences are defined as 'ON ⇒ OFF ⇒ ON' and 'ON ⇒ OFF ⇒ OFF ⇒ ON', respectively (see METHODS-

208 *Fraction of period* section). We mathematically determined the states of On and Off in
209 each year for individual trees with $ON_i(t)$ and the spatial distributions of $ON_i(t)$ for
210 6 years are displayed in Fig.4-a-f. Wild tree spaces, generally have a wide-ranged
211 spectrum of periods in which variable periods such as period-two, period-three, period-
212 four, and more, including aperiodic motions, exist. For example, period-three was
213 dominant for *Zerkova serrata* but period-four and period-five were non-trivial. For tree
214 crops, their synchronisations occurred generally on a two-year cycle (i.e. period-two),
215 which is why "alternate" bearing and/or "biennial" bearing has become common
216 terminology in pomology[1]. Using the fractions of periods *FR*(*Q*) (see METHODS-
217 *Fraction of period* section), we successfully display the spatial distributions of the
218 compositions of period-two, period-three, period-four and period-five for individual
219 trees of the orchard (Fig. 4-g-j). Figures 4(g) and (j) indicate the fractions of period-two,
220 period-three, period-four and period-five, which are *FR*(2) = 0.517, *FR*(3) = 0.103,
221 *FR*(4)=0.0244 and *FR*(5)=0.0060,respectively. Obviously, Period-two is dominant in the
222 orchard. However, from a farm management point of view, it is informative to identify
223 those trees whose cycles are three years ,four years or five-years. For example, in the
224 eastern area, the fraction of period-two (*FR*(2)) is smaller than that in the west; further,
225 the fraction of period-three (*FR*(3)) in the east is larger than that in the west. For another
226 example, from the 9,562 trees, we can identify 57 trees whose period are five-years and
227 investigate why they behave in this unique manner.
228 The results from the novel approach applied to the yield data of the orchard uncover
229 unique and important features of the phase synchronisations in the orchards:
230 (1) The gradient of the strength of in-phase synchronisation from west to east.
231 (2) The occurrence of perfect synchronisation in the whole orchard.

232 (3) The spatio-temporal transition from order (perfect in-phase synchronisation) to
233 disorder (desynchronisation).
234 To infer from these findings and explain the observed phase synchronisation, we
235 developed a model. The structure of the model was a network of oscillators, which were
236 the RBMs for all the trees; a common noise (external force) $e_C(t)$ was identically
237 imposed on all the trees in each year *t*. We employed diffusive coupling as the direct
238 coupling of the network and considered the coupling timing in the growth stage of a
239 plant. The detail of the model is given in the METHODS- *model development section*)
240
241 **Essential factors in the spatial synchronisation of the orchard**
242 **Fig**ure 5 shows that the common noise, local coupling, and gradient of the cropping
243 coefficient are essential factors

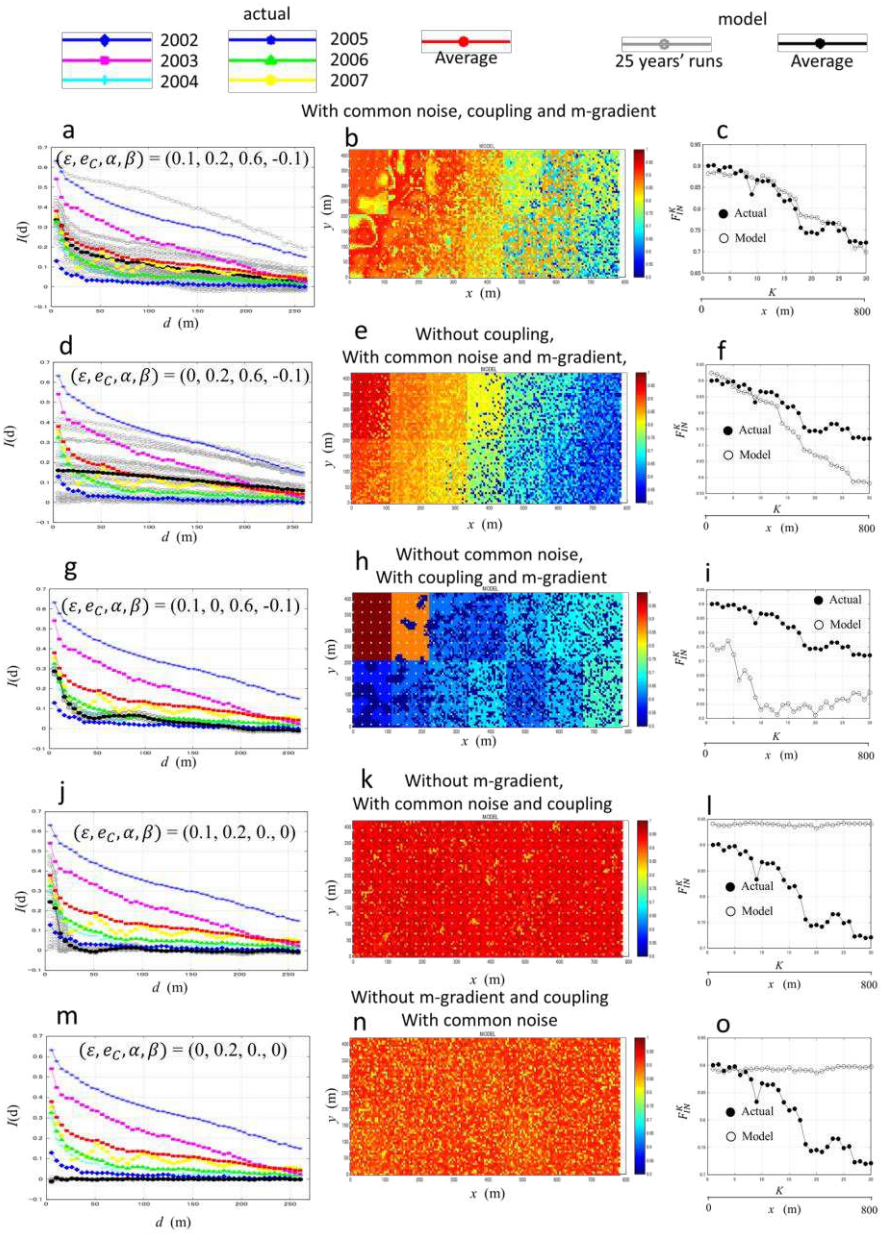

Figure 5. Demonstration of the long-ranged spatial correlations and spatial distribution of phase synchronisation realised by diffusive coupling and common noise.

The parameter settings used for the numerical simulations are as follows: The first row :with the three essential factors $(\varepsilon, e_C, \alpha, \beta)$ = (0.1, 0.2, 0.6, -0.1), The second row : without common noise $(\varepsilon, e_C, \alpha, \beta)$ = (0, 0.2, 0.6, -0.1), The third row : without the local direct coupling $(\varepsilon, e_C, \alpha, \beta)$ = (0.1, 0, 0.6, -0.1), The fourth row : without the spatial gradient of cropping coefficients $(\varepsilon, e_C, \alpha, \beta)$ = (0.1, 0.2, 0, 0) , and the fifth row : only with common noise $(\varepsilon, e_C, \alpha, \beta)$ = (0, 0.2, 0, 0).

253 Given the combinations of the essential parameters (ε, e_C,α,β), the best fit common
254 noise (external force) $e_C(t)$ and initial values of $S_i(1)$ (i = 1, 2, …, 9,562) for 25-year
255 periods are determined as follows. The initial values of $S_i(1)$ for 9,562 trees are given by
256 normal distribution [μ,σ] = [L_T-P_0, e_C] = [90, 0.2]. The model runs until t becomes 500
257 and the best fit 25 years period in terms of $F_{I\mathbb{N}}^{K}$ (K=1,2,…,30) is subsequently selected.
258 The spatial correlation I(d) diagrams and the spatial distribution of f_{in}^{i} maps are
259 exhibited in the left column and the right column, respectively.
260 According to the above three findings, the results, and previous work, we assume that
261 (a) the Common noise (external force) (e_C), (b) gradient of cropping coefficient (m),
262 and (c) direct coupling (ε) as the three essential factors implemented in the model. The
263 range of coupling is set r=13 m so that one tree coupled with neighbouring twelve trees
264 at most.
265 Three characteristics of the spatial correlation are observed in the orchard: (i)
266 high short-range spatial correlation, (ii) significant long-range spatial correlation, and
267 (iii) wide range variation of $I(d)$ on the time domain.
268 In this section, we validate the effects of the three parameters on phase synchronisation
269 by considering the characteristics of the spatial correlation.
270 Numerical experiments with the developed model were conducted to investigate the
271 effect of the essential factors in terms of I(d). Here, we use $I(d)$, known as Moran's I, as
272 the index of the spatial correlation[39], and the map of f_{in}^{i} (Fig.5(b)) to compare with the
273 real data shown in Fig.1-(a). Five different values of the set $(\varepsilon, e_C, \alpha, \beta)$ were tested
274 (Fig. 5). m and ε are the control parameters of the network model and e_C is the
275 common noise (environmental external force) that generates the phase synchronisation.

276 α and β are the spatial gradients of m in west-east and south-north directions,
277 respectively. Based on a preliminary parameter study (see S-1), we estimated the values
278 for the essential factors as $e_C = 0.2$, $\varepsilon = 0.1$ and $m = R_0 + \alpha x/L_{WE} + \beta y/L_{WE}$ (R_0 =1.1, α =
279 0.6 and $\beta = -0.1$) i.e. $(\varepsilon, e_C, \alpha, \beta) = (0.1, 0.2, 0.6, -0.1)$ for Fig. 5(a)-(c). In this case,
280 the spatial correlations ($I(d)$) of the model satisfies the three characteristics of the
281 orchard as follows (i) for short-range spatial correlation, $I(d)$ is up to 0.64 at d = 5.2 m,
282 (ii) for long-range spatial correlation, $I(d)$ is larger than 0.37 at d = 100 m, and (iii) $I(d)$
283 fluctuates widely over the same range. The map of $f_{\mathrm{in}}^{\mathrm{i}}$ (Fig.5(b)) shows good
284 agreement with that of the real data shown in Fig.1-(a), and the actual and model plots
285 of F_{IN}^{K} plots (Fig.5(c)) also shows good agreement. In the absence of coupling (second
286 row), the short range spatial correlation (Fig. 5(d)) is much smaller than that of the
287 presence of coupling case (Fig.5(a)), while the map of $f_{\mathrm{in}}^{\mathrm{i}}$ (Fig.5(e)) and the actual
288 and model of F_{IN}^{K} plots (Fig.5(f) show some agreement with the real data in the western
289 area, but not the eastern area. Without common noise case (third row), in Fig.5(g), the
290 short-range correlation is as high as 0.3 because of the local direct coupling (ε=0.1).
291 However, all the $I(d)$s rapidly drop to zero when d = 20 m, and there is no long-range
292 spatial correlation and no yearly fluctuation in $I(d)$. The map of $f_{\mathrm{in}}^{\mathrm{i}}$ and the actual and
293 model of F_{IN}^{K} plots indicate that there is no significant phase synchronization over the
294 entire orchard (Fig.5(h) and (i)). These results suggest that common noise is
295 indispensable as an external force and the synchronization observed in the orchard
296 (Fig.5) should be a type of common noise induce synchronisation.
297 As the cropping efficiency gradient is given by $m = R_0 + \alpha x/L_{WE} + \beta y/L_{SN}$, the
298 absence of m-gradient is implemented by setting $\alpha = \beta = 0$,therefore, m is 1.1 over the

orchard. In this case of without the spatial gradient of the cropping efficiency (Fig.5(j)), very strong short-range spatial correlation, $I(d) = 0.98$ exists at $d = 5.2$ m; however, there is no long-range spatial correlation. Figure 5-(k) and (l) exhibits the spatial phase synchronization with $f_{\mathrm{in}}^{\mathrm{i}} = 1$ over the entire orchard and for 25 years. The results of Figs. 5(j)-(l) suggest that even with the presence of both the common noise (e_C) and coupling (ε), the gradient of m is still necessary to explain the features of long-range spatial correlations and spatial distribution of phase synchronisation in the orchard as observed in Fig.1. The last case is the one with only common noise (i.e. no coupling and no m-gradient). There is no spatial correlation (Fig.5(m)). The map of $f_{\mathrm{in}}^{\mathrm{i}}$ and the actual vs. model plot indicates that the same high synchronization intensity (around 0.9) as in the west is distributed throughout the orchard (Fig.5(n) and (o)). In an orchard which is newly planted and there is no m-gradient, the feature demonstrated in Fig.5(m)-(o) could be happen in a real case.

Numerical interpretation of the experimental results: How endogenous dynamics and exogenous force generate variable types of phase synchronisations

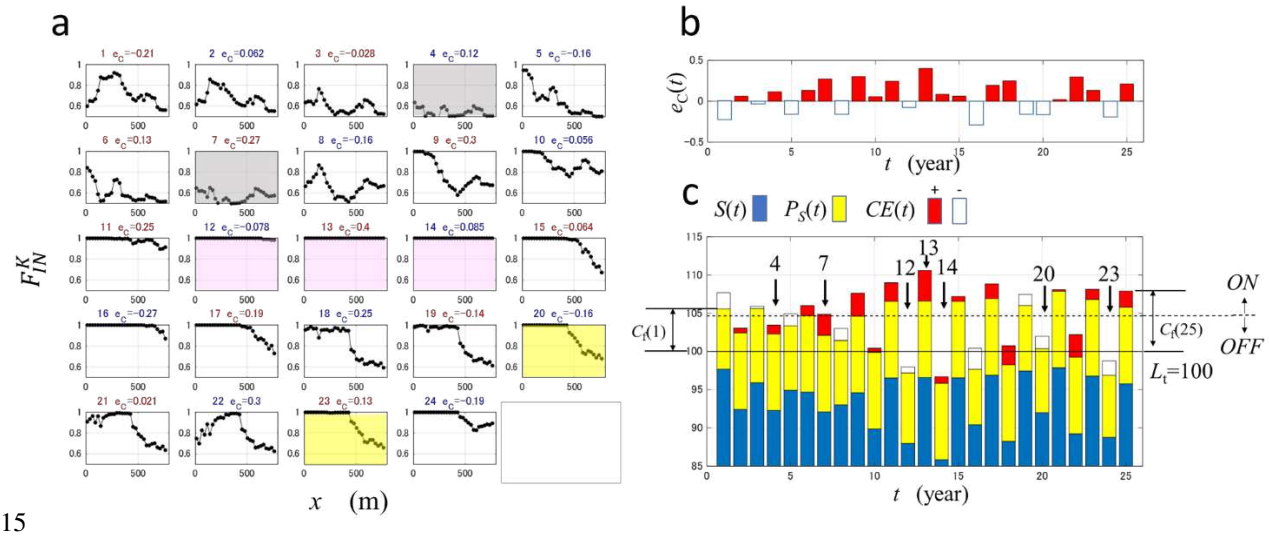

315

316 Figure 6. Spatio-temporal behaviour of phase synchronisations caused by endogenous dynamics with
317 exogenous force. The numerical experiments were conducted with the best fit external force
318 (common noise) $e_C(t)$ and initial values of $S_i(1)$ (i = 1, 2, …, 9,562) determined in Fig.5-(b) and
319 calculated 24 $F_{IN}^K(t)$ and $F_{IN}(t)$. $(\varepsilon, e_C, \alpha, \beta) = (0.1, 0.2, 0.6, -0.1)$

320 (a) 24 $F_{IN}^K(t)$ values are displayed for t=1,2,…24 determined from 25 years runs.
321 (b) The time (year) history of external force (common noise) $e_C(t)$. t=1,2,…25. "red" and
322 "white" correspond to positive and negative values of $e_C(t)$.
323 (c) $S(t) = \frac{1}{N}\sum_{i=1}^{N} S^i(t), N = 9.562$ represents the total amount of resource reserves of all trees at
324 year *t*. $P_S(t)$ is the total resource added on all trees at year *t*. $CE(t) = P_0 \times e_C(t)$ is the external
325 force (common noise) identically imposed on all trees at year *t*. In the bar chart, "red" and "white"
326 correspond to positive and negative effects of external forces (common noise); $CE(t)$, respectively.
327 The excess of the threshold (L_t=100) of the total amount of $S(t)$, $P_S(t)$, and $CE(t)$ becomes the
328 flowering cost $C_f(t)$.

329

330 Using the model with the estimated parameters ; $(\varepsilon, e_C, \alpha, \beta) = (0.1, 0.2, 0.6, -0.1)$
331 demonstrated in Fig.5-(a) and (b), Fig.6 exhibits how endogenous dynamics and
332 exogenous force generate variable types of phase synchronisations. Figure 6-(a) shows
333 the spatial distribution of $F_{IN}^K(t)$ of the model. The mode alternative transitions
334 between order and disorder in both space and time (annual) domains were the

substantial nature of the dynamics and important behaviour in terms of phase synchronisation.

Resource switching and weather cues act together to cause synchronisation such as masting and alternate bearing (Lyles et al. 2009)[7]. The results described in Fig. 6 confirm this knowledge mathematically. The combination of endogenous dynamics and exogenous forces cause the perfect phase synchronisations. Figure 6(a) displays the $F_{IN}^{K}(\mathrm{t})$ for 25 years. An interesting finding of this analysis is that significantly strong phase synchronisations generally occur when the common noise (external force) is high; however, this is not always the case. Furthermore, almost complete desynchronisation occurs even when a significantly large common noise (external force) is present. The perfect phase synchronisations occur when t = 12, 13, and 14 with $F_{IN}(\mathrm{t}) \geq 0.997$ (i.e. $F_{IN}(12) = 0.9975, F_{IN}(13) = 1.0, \text{and } F_{IN}(14) = 1.0$). The almost complete desynchronisations occur when t = 4 and 7 with $F_{IN}(\mathrm{t}) \leq 0.58$.

Three consecutive perfect in-phase synchronisations occur when t = 12, 13, and 14; t = 13 is an "off-year" as the year (t=12) is the second largest "on-year" within 25 years; thus, the production ($C_{\mathrm{f}}(12)$) was zero, because the excess of the threshold (L_{t}=100) of the total amount of $S(\mathrm{t})$, $P_{\mathrm{S}}(\mathrm{t})$, and $CE(\mathrm{t})$ becomes the flowering cost $C_{\mathrm{f}}(\mathrm{t})$ which is proportional to the production $C_{\mathrm{a}}(\mathrm{t})$. Consequently, the resource remained in the bodies of the tree, meaning that S (13) nearly obtained the almost maximum value for all trees. Additionally, that year (t=13) had the best condition as $e_{\mathrm{C}}(13)$=0.4 ($CE(13)$=4) within 25 years, which allowed all the trees to change their states into the maximum on-year state with the perfect in-phase synchronisation (in fact $F_{IN}(13) = 1.0$). As a result, the smallest amount of resources remained in the bodies of the trees meaning that S (14) obtained the minimum value within 25 years (see Fig.6(c) at t=14). The external force

was not large ($CE(14)=2$) with no excess (i.e. $C_f(14)=0$) for all trees so that the perfect synchronisation ($F_{IN}(13) = 1.0$) still remained in "off-year" state. Thus, three consecutive perfect phase synchronisations in other words, this is the mechanism of the three years consecutive perfect phase synchronisations (i.e. three years mode locking)). If $CE(14)$ is at least greater than 6, t=14 will be a weak "on-year" state with partial desynchronization and this mode lock will terminate.

In the opposite case, t=6 was an "on-year" with a weak synchronisation mode (see Fig.6(a)), t=7 should be succeeded by "off-year" if $CE(7)$ was a normal value. However, $CE(7)$ was large enough (i.e. $CE(7)$ =3.5 is the second largest within 25 years,) to keep very weak "on-year" and the model turned to the almost complete desynchronization ($F_{IN}(7) = 0.568$). It is interesting to note that the simulation results show that such a large external force causes desynchronization instead of synchronization.

Owing to the historically imposed exogenous forces (accumulated footprints of exogenous forces) on the endogenous dynamics, a mode-locking emerged. We note that two types of "in-phase mode-locking" exist, one which occurred in the "off-year" and another which occurred in the "on-year". The first one occurred at t = 12 and 14, and the second one occurred at t = 13. Also two types of "desynchronization mode" exist, one which occurred in the "off-year" and another which occurred in the "on-year", occurred at t=4 and t=7, respectively. The perfect in-phase synchronisation (order) and perfect desynchronisation (disorder) were the two extremes. Most of the modes of phase synchronisation appeared either in between or were mixtures of both extremes e.g. Fig.6.(a) at t=20 and 23. The mode of the mixture may be considered as a "chimaera like state", which was first experimentally captured in optical-coupled map lattices in

nonlinear physics[40]. Here, we detected the "chimera like state" in the field experiments of the orchard in 2004-2005 period as shown in Fig.2(h).

DISCUSSIONS

The population dynamics of chaotic oscillators is a universal phenomenon of interest in several fields. It has been employed to treat and understand the synchronisation phenomenon of perennial plant populations as mathematical spatio-temporal dynamics in nonlinear physics. This synchronisation phenomenon is also of practical importance in food production, forest production, and ecosystem management. In this study, we assumed that the synchronisation of 9,562 pistachio trees was "a common noise induced synchronisation" in chaotic oscillator networks with local diffusion coupling. By proposing the method of detecting the synchronisation intensity at the population level and individual level, we successfully visualised the spatial distribution of the synchronisation with real data and verified the mathematical model.

The gradient of the strength of phase synchrony is a unique feature of the orchard. The results led us to one conclusion: the cropping coefficient (m) increases from 1 to 1.6 from the western part to the eastern part of the orchard over a distance of 780 m. The cropping coefficient m is the product of the cost ratio R_C and fertility successes Z. R_C is the control parameter of the RBM (e.g. -R_C is the slope at the fix point of the RBM) ; it might be hard to imagine that R_C changes from 1 to 1.6 in a population of clone plants. The fertility successes Z, however, are positively relevant to the pollen density. In the pistachio orchard, male trees are evenly located; thus the pollen density is uniform and the soil type is also uniform with a small geographical slope. It is also hard

406 to assume that Z changes from 1 to 1.6 in the west to east of the orchard. Therefore, the
407 source of the gradient of the cropping coefficient m remains an open question. In
408 California, the westerlies might be a candidate source, if the westerlies carry a sufficient
409 amount of pollen from west to east, resulting in the pollen density increasing coherently
410 in a west-east direction in the orchard. This hypothesis must to be validated by intensive
411 field survey of pollen drifting due to the westerlies.
412
413 This paper hypothesise that the cause of local coupling is underground interaction
414 between trees through root grafting/mycorrhizal networks as direct-coupling [17,27]. It is a
415 key factor that could explain the long-range spatial correlation of the orchard. By setting
416 the appropriate timing of the direct coupling in the growth stage of a plant, the diffusive
417 coupling of RBMs works to enhance the in-phase synchronisation. This model is
418 designed to realise the dynamics derived from the hypothesis.-In the numerical
419 experiments of Fig. 4, the best fit range of direct coupling was 15 m. This implies that
420 direct coupling of root grafting had a range of 26 m. Nevertheless, it is necessary to
421 conduct a field survey to confirm this explanation. Beside the direct local coupling
422 hypothesized here, there is another possible hypothesis that local (spatial) variability of
423 pollen density, soil fertility and/or irrigation for in-direct local coupling. This in-direct
424 local coupling hypothesis should be an interesting future work to deepen our
425 understanding agro-ecological systems.
426
427 For suppressing the alternate bearing, the strength of the phase synchronisation in the
428 orchard should be reduced. For example, if the spatial gradient of the phase
429 synchronisation occurs because of the pollen density, the number of male trees in the

western area can be increased to ease the alternate bearing. For another example, if the direct coupling caused by the natural root grafting and/or mycorrhizal networks enhances the phase synchronisation, breaking the root networks using a subsoiler or pan-breaker can help remediate the alternate bearing. Thus, clarifying the mechanism of the spatial gradient *m* is important for farm management.

Observing the trends of on-off cycle in circle maps expressed in Fig.3 and , it is empirically reasonable to predict 2008 is an “off-year”. The dominant two year circle demonstrated in Fig.4 also suggests that 2008 might be an “off-year”. In fact, as shown in S-2, in King's county where the orchard locates, 2008 was an “off-year” . This static data (S-2) are consistent with the empirical prediction. This is the advantage of the circle maps (Fig.3) and fraction of periods (Fig.4) in terms of yield prediction. However, with this empirical approach, we cannot predict yield at individual tree level. Sakai and Noguchi (2008) developed the ensemble reconstruction technique (ERT) to reconstruct a possible collective dynamics of the population of 7 years and 48 unshiu citrus trees [41,42]. They applied the deterministic nonlinear prediction (NDP) method [43-45] on the reconstructed dynamics to make successful one year forward yield prediction of individual trees and the population. As the size of their data used and the strength of synchronisation of the citrus population were much smaller than that of the data of this study. In future studies, the same method (DNP combined with ERT) can be expected to predict the yield one year ahead for individuals in this orchard.

This is challenging in terms of both nonlinear physics and farming operations. In orchards and forests, the uniformity of individual trees is ensured, and accurate spatial arrangement information can be easily obtained. Therefore, the proposed approach can

be applied to tree crops other than pistachio and forest trees. In other words, nonlinear physics is useful in fruit production, tree production, and ecosystem management and is expected to be widely applied to these fields.

METHODS

Field experiments

In the orchard with $N = 9{,}562$ (Fig. 1), the male pistachio trees were evenly spaced (26 m × 26 m); female trees were located within 14 m of the nearest male tree to receive enough pollen. The data were obtained from a 32.3-ha (416 m × 777 m) orchard located at 35° 86′ N, 119° 87′ W (Lost Hills, Kings County, California, USA)[7-9]. The trees were spaced 5.2 m and 6.4 m in rows and columns, respectively. In 2007, the trees in the western part of the orchard were removed, so the total area of the orchard was 22.7 ha[17]. Synchronisation was exhibited in the annual yield, called alternate bearing, for 2002–2007. The data used here is available as a summplimentary dataset. The subset data excluding blank and missing data points from the data is available[17].

In-phase/out-of-phase analysis technique

Fraction of in-phase/out-of-phase. The phase synchronisation of a population comprises two classes: in-phase and out-of-phase[15]. Let $x_i(t)$ be the yield of the ith tree in year t, and $\emptyset(\mathrm{i},\mathrm{j},t)$ be the phase between the ith and jth trees,

$$\emptyset(i,j,t) = \{x_i(t+1) - x_i(t)\}\{x_j(t+1) - x_j(t)\}. \quad (3)$$

Then, the fraction of the in-phase behaviour of tree i relative to the remaining trees in the population (size N) in year t is defined as

$$f_{in}^{i}(t) = \frac{1}{N-1}\sum_{j=1,j\neq i}^{N} H(\emptyset(i,j,t)); \quad (4)$$

that is, $f_{IN}^{i}(t)$ is the ratio of tree i[th] to be in-phase relative to the rest of the *N*-1 trees in the population. We denote by f_{IN}^{i} the time average of $f_{IN}^{i}(t)$ for tree *i*. The fraction with in-phase behaviour $F_{IN}(t)$ within the population (size *N*) for year *t* is calculated from

$$F_{\mathrm{IN}}(t) = \frac{1}{\mathrm{N(N-1)}}\sum_{i=1}^{\mathrm{N}}\sum_{j=1,j\neq \mathrm{i}}^{\mathrm{N}} f_{\mathrm{IN}}^{i,j}(t) \quad (5)$$

$f_{IN}^{i}(t)$ and $F_{\mathrm{IN}}(t)$ quantify the strength (rate) of phase synchronisation for the individual tree and population, respectively.

$F_{IN}^{K}(t)$ (K = 1, 2, ..., 30) is the west-east directional averages of $f_{in}^{i}(t)$ for every 5 columns. $F_{IN}^{L}(t)$ (L = 1, 2, ..., 9) is the south-north directional averages $f_{in}^{i}(t)$ for every 9 rows, respectively. F_{IN}^{K} and F_{IN}^{L} are the time (year) averages of $F_{IN}^{K}(t)$ and $F_{IN}^{L}(t)$, respectively.

Perfect in-phase synchronisation is when F_{IN} any size of the population and represents "order". In the case of a population whose size is larger enough, F_{IN}=0.5 indicates all trees behaving completely randomly (i.e. perfect out-of-phase synchronisation) and represents "disorder".

Fraction of period[16]. A period-Q sequence is defined as the sequence where one 'on-year' at *t* is followed by Q-1 'off-years' and an 'on-year' arises at t + Q. The fraction of period-Q of $x_i(t)$ is determined by

$$FP_i(Q) = \frac{Q}{(T-1)-mod(T-1,Q)}\sum_{t=1}^{T-Q}[ON_i(t)ON_i(t+Q)\prod_{j=1}^{Q-1}\{1-ON_i(t+j)\}]. \quad (6)$$

where, $ON(t) = \begin{cases} 1 & x_i(t) > \bar{x}_i, \quad "on-year" \\ 0 & x_i(t) \le \bar{x}_i, \quad "off-year" \end{cases}$, and $\bar{x}_i = \frac{1}{T}\sum_{t=1}^{T} x_i(t)$.

The phase angle $\theta(t)$ of a single time series $x(t)$ is given by

$$\theta(t) = \text{angle}(HT[X(t) - \bar{X}]), \tag{7}$$

where HT is the Hilbert transform of the true signal $X(t)$ and $\bar{X}$ is the time average of $X(t)$.

Moran's I. Moran's I is the distance measure of the spatial correlation,

$$I(d) = \frac{N}{W}\frac{\sum_{i=1}^{N}\sum_{k}^{N} w(i,k)[x_i(t)-\bar{x}(t)][x_k(t)-\bar{x}(t)]}{\sum_i [x_i(t)-\bar{x}(t)]^2}, \tag{8}$$

where N denotes the number of spatial units indexed by i and k; x_i the yield, x the mean of the yield, $w(i,k)$ a matrix of spatial weights with zeros on the diagonal (i = 1,…, N; $w(i, i) = 0$); here, W is the sum over all w(i,k).

$$w(i,k) = \begin{cases} 1 & |D(i,k) - r| \le \Delta d \\ 0 & |D(i,k) - r| > \Delta d \end{cases}, \tag{9}$$

where $D(i,k)$ denotes the distance between tree i and tree k.

Model development

The tent map, global coupled map (GCM), local coupled map (LCM), and coupled map lattices (CML), and common noise induced synchronisation (CNIS) are all fundamental models in nonlinear physics[22-25]. To understand the spatial synchronisations observed in the orchard, we introduce a novel model here. This model combines CML and CNIS by implementing direct coupling RBMs networks with imposing external force on all trees identically. These popular models in nonlinear physics are also useful for explaining the spatio-temporal collective dynamics in ecological systems.

Networks of plants. In addition to the oscillator, we also use the RBM, which is a one-dimensional tent map for a single tree for masting and alternate bearing[18]. $S^i(t)$ represents the amount of resource reserves at the beginning of year t for tree i, $P_S(t)$ the additional resource (e.g. photosynthetic residue[18] or unspecified substances[46-47]) being accumulated by flowering season in the trunk of a plant, and L_t the upper limit of the pool in which the resource is reserved in the plant body.

Direct Coupling. The common way of diffusive coupling[21] on RBMs generates out-of-phase behaviour[15]. Conversely, here, to enhance the in-phase synchrony, we implement the coupling in a novel form as

$$SA^i(t) = S^i(t) + \frac{1}{N-1}\sum_{j\neq i}^{N} \varepsilon_{j,i}\left[S^j(t) - S^i(t)\right] \ , \tag{10}$$

where $\varepsilon_{j,i}$ is the coupling strength and $SA^i(t)$ is the amount of resource when material exchanges occur. Thus, we assume that material exchanges occur underground before flowering.

The map G: $S^i(t+1) \to S^i(t+1)$ is

$$S^i(t+1) = \begin{cases} SA^i(t) + P_S(t) - C_f^i(t) - C_a^i(t), & SA^i(t) + P_S(t) > L_t \ \ "on-year" \\ SA^i(t) + P_S(t), & SA^i(t) + P_S(t) \leq L_t \ \ "off-year" \end{cases} \tag{11}$$

in which the cost of flowering $C_f^i(t)$ and the cost of fruiting are given by

$$C_f^i(t) = \begin{cases} SA^i(t) + P_S(t) - L_t & SA^i(t) + P_S(t) > L_t \\ 0 & SA^i(t) + P_S(t) \leq L_t \end{cases} , \tag{12}$$

and,

$$C_a^i(t) = mC_f^i(t). \tag{13}$$

where *m* is the cropping efficiency given by the product of the cost ratio R_C and fertility successes Z.

$$m = R_C Z. \tag{14}$$

We assume *m* varies from tree to tree in the orchard,

$$m_i = R_0 + \alpha x_i / L_{WE} + \beta y_i / L_{SN}, \tag{15}$$

where (x_i, y_i) are the spatial coordinates of the i^{th} tree. L_{WE}, and L_{SN} are the distances from the west end to east end and the south end to north end of the orchard, respectively.

External force (common noise): Common noise is *CE*(t) the external environmental force imposed on all trees identically. *CE*(t) is addied on $P_S(t)$, that is,

$$CE(t) = e_C \sigma(t), \tag{16}$$

$$P_S(t) = P_0\{1 + CE(t)\}, \tag{17}$$

where P_0 denotes the intrinsic annual surplus and $\sigma(t)$ is the normal distribution $\mathrm{N}(\mu, \sigma^2) = \mathrm{N}(0,1)$. The level of common noise is represented by e_C.

SUPPLEMENTS

S-1. Preliminary parameter study

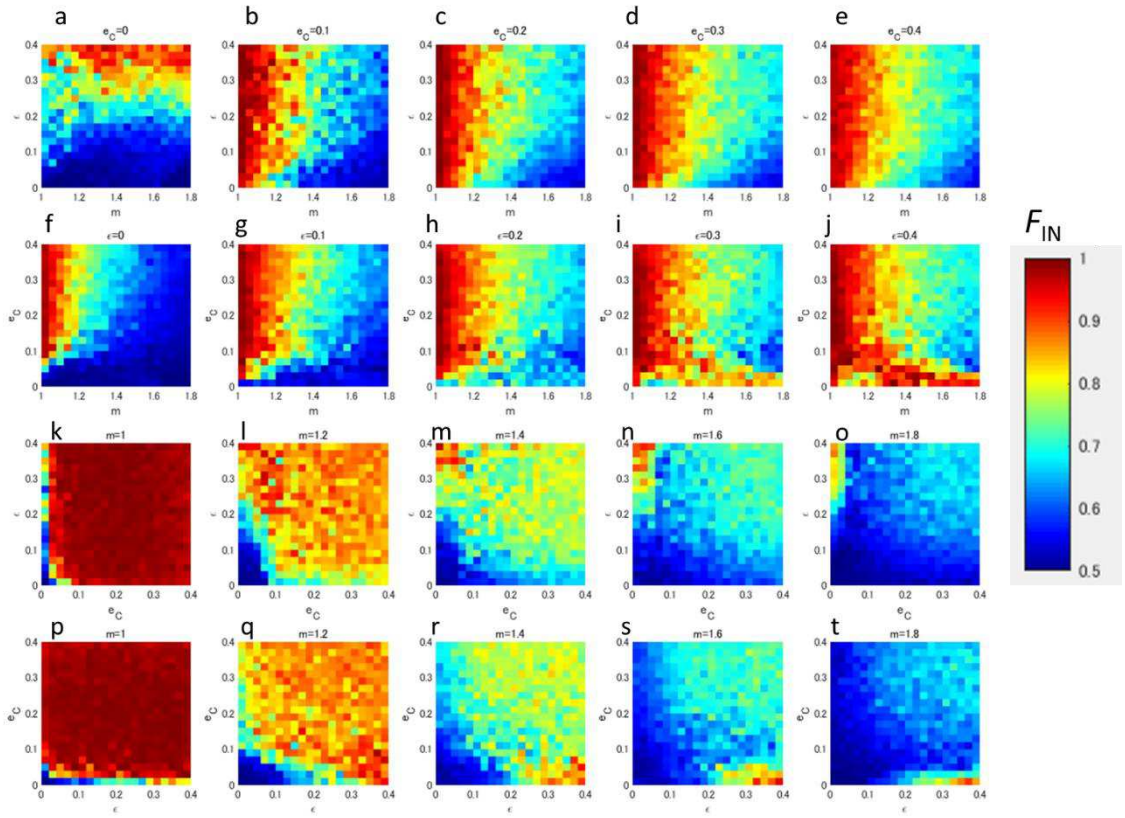

Figure S-1. Dependence of the strength of in-phase synchronisation on m, ε and e_C. First row (a), (b), (c), (d), and (e):m *vs* ε diagram for e_C=0, 01, 0.2, 0.3,and 0.4; second row (f), (g), (h),(j) , and (k):m *vs* e_C diagram for ε=0, 01, 0.2, 0.3, and 0.4; third row (k) ,(l), (m), (n) , and (o): e_C $vs.\varepsilon$ diagram for m = 1.0, 1.2, 1.4, 1.6, and 1.8.; fourth row (p),(q), (r),(s) , and (t): e_C $vs.\varepsilon$ diagram for m = 1.0, 1.2, 1.4, 1.6, and 1.8.

Fig. S-1 shows the preliminary parameter study for the essential factors.

In the orchard, F_{IN} ranges from 0.92 to 0.7 in the west-east direction. As shown in the panels of the third and last rows, both e_C and ε do not affect the F_{IN} range of the orchard (i.e. F_{IN} =[0.92, 0.7]). Since m is the only parameter changing F_{IN} in that range

573 (i.e. 0.92 to 0.7), we assume that m changes spatially from west to east. The cropping
574 coefficient m is the control parameter of the RBM, which depends on plant species.
575 Common noise e_C and the local direct coupling ε vary depending on meteorological
576 environments and the state of the root network developments of the orchards,
577 respectively. Therefore, F_{IN} is considered as a function of m accompanied with
578 endogenous and exogenous parameters; ε and e_C respectively. For all panels of Fig. S-
579 1, the phase synchronisations are enhanced by local coupling ε. As exhibited in Figs. S-
580 1(f) and (g) later, ε larger than 0.2 cannot satisfy the feature observed in the spatial
581 correlation of the orchard. Common noise e_C enhances phase synchronisation,
582 however, an e_C higher than 0.2 does not increase F_{IN} significantly.
583 Summarising the results and considerations above, we estimate the ranges of the three
584 essential parameters i.e. common noise (e_C = 0.2~0.3), local coupling (ε = 0.1) and
585 cropping coefficient (m = 1~1.6, west to east) as general approximation values.
586
587

S.2 Total production of the orchard and King's county

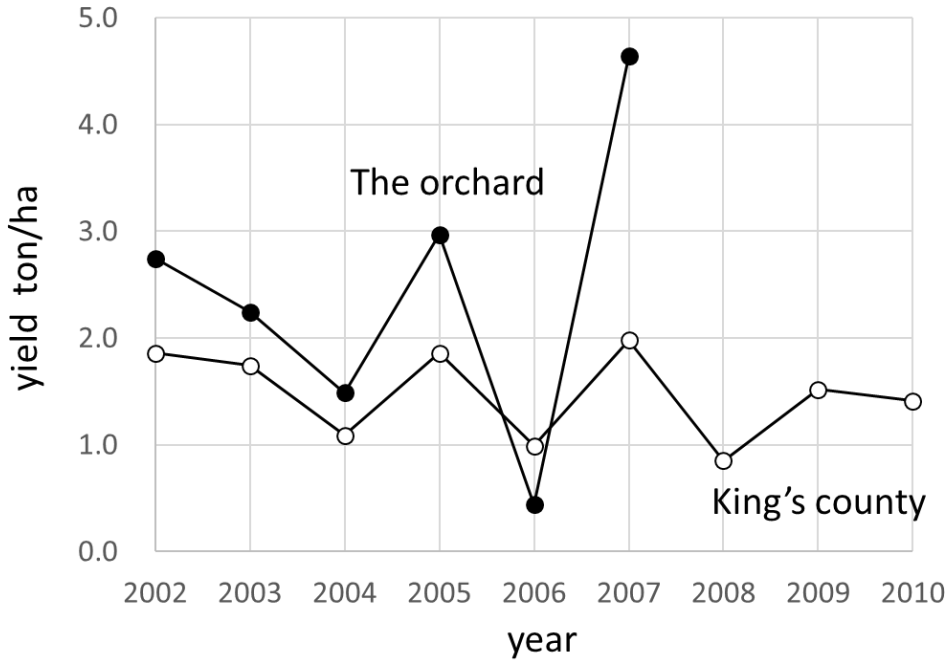

S-2 Total productions of the orchard and King's county

In the six-year measurement period (2002-2007), the abundance of both species is consistent. It is reasonable to assume that 2008 is a good year.

Acknowledgements

K.S thanks Prof. Eliezer Goldschmid (emeritus professor of agriculture at the Hebrew University of Jerusalem), Prof. Awadesh Prasad (Department of Physics and Astrophysics, University of Delhi) and Prof. Rajarshi Roy (Institute for Research in Electronics and Applied Physics, University of Maryland) for productive conversations. KS also thanks JSPS Grant-in-Aid Nos. 23380152, and 16K15016. AH acknowledges NSF DMS – 1840221 NSF DMS – 184022.

Author Contributions

K.S., P.B.,S.U and A.H. conceived the research. P.B. and R.T. designed the field survey and performed measurements and established the data set. K.S. conducted the numerical simulations and the analysis of the results, and prepared the manuscript. All of them participated in discussions and provided intensive suggestions for improving the manuscript.

Correspondence to Kenshi Sakai.

Email: ken@cc.tuat.ac.jp

Ethics declarations

Competing interests

The authors declare no competing interests.

Data Availability

The data are available in the SUPPLEMENTS section.

623 **References**

624 [1] Goldschmidt, Eliezer E. Plant grafting: new mechanisms, evolutionary implications.
625 Front. Plant Sci. **5**, 2014.00727,2014

626 [2] Sakai, K. Nonlinear dynamics and chaos in agriculture systems, (Elsevier Science,
627 Amsterdam, 2001).

628 [3] Prasad, A. & Sakai, K. Understanding the alternate bearing phenomenon: Resource
629 budget model. Chaos **25**, 123102-6 (2015).

630 [4] Li, C-Y.,Weiss,D., Goldshmidtm,E.E. Girdling Affects Carbohydrate-related Gene
631 Expression in Leaves, Bark and Roots of Alternate-bearing Citrus Trees. Ann. Bot.
632 **92**(1), 137–143(2003).

633 [5] Kon, T.M. & Schupp, J.R. Apple crop load management with special focus on early
634 thinning strategies: a US perspective. Hortic. Reviews. **46**, 255–298 (2019).

635 [6] Khalil, S.K.et al. Foliar ethephon fruit thinning improves nut quality and could
636 manage alternate bearing in pecan. Pharm. Chem. J. **3**,150–156 (2016).

637 [7] Lyles, D., Rosenstock, T. S, Hastings, A., Brown P. H. The role of large
638 environmental noise in masting: General model and example from pistachio trees. J.
639 Theor. Biol. **259**(4), 701–713 (2009).

640 [8] Rosenstock, T. S., Rosa, U.A., Plant, R. E. & Brown P. H. A reevaluation of alternate
641 bearing in pistachio. Scientia Horticulture **124**,149–152 (2010).

642 [9] Rosenstock T. S., Hastings, A., Koenig, W. D., Lyles, D.J. & Brown P. H. Testing
643 Moran' s theorem in an agroecosystem. Oikos **120**,1434–1440 (2011).

644 [10] Koenig, W. D. & Knopes, J. M. H. The mystery of masting in trees. American
645 Scientist **93**, 340-347 (2005).

[11] Kelly, D. & Sork, V. L. Mast seeding in perennial plants: why, how, where? Annu. Rev. Ecol. Syst. **33**, 427-447 (2002).

[12] Satake A. & Iwasa, Y. Pollen Coupling of Forest Trees: Forming Synchronized and Periodic Reproduction out of Chaos. J. Theor. Biol. **203**,63-84 (2000).

[13] Satake A. & Iwasa, Y. The synchronized and intermittent reproduction of forest trees is mediated by the Moran effect, only in association with pollen coupling. J. Ecology **90**, 830-838 (2002).

[14] Satake A, & Iwasa Y. Spatially limited pollen exchange and a long-range synchronisation of trees. Ecology **83**, 993–1005 (2002).

[15] Prasad,A., Sakai,K,. & Hoshino,Y. Direct coupling: a possible strategy to control fruit production in alternate bearing. Sci. Rep. **7**, 39890 (2017)

[16] Sakai, K., Hoshino, Y., Prasad, A., Fukamachi, A. & Ishibashi, A. Period-3 dominant phase synchronisation of Zelkova serrata: n order-collision bifurcation observed in a plant population. Sci. Rep. **9**,15568 (2019)

[17] Noble A.E., Rosenstock, T. S., Brown, P.B., Machta, J. & Hastings, A. Spatial patterns of tree yield explained by endogenous forces through a correspondence between the Ising model and ecology. PNAS.**115** (8) ,1825-1830 (2018)

[18] Isagi, Y., Sugimura, K., Sumida, A. & Ito, H. How does masting happen and synchronize? J. Theor. Biol. **187**, 231-239 (1997).

[19] Akita, T., Sakai, K., Iwabuchi, Y., Hoshino, Y., & Ye, X. Spatial autocorrelation in masting phenomena of Quercus serrata detected by multi-spectral imaging. Ecol Model **215**(1-3), 217-224 (2008).

[20] Crone,E.E. & Rap.J.M. Resource depletion, pollen coupling, and the ecology of mast seeding. Ann. N.Y. Acad. Sci. **1322** , 21–34 (2014).

[21] Noble A.E., Machta, J.& Hastings, A. Emergent long-range synchronisation of oscillating ecological populations without external forcing described by Ising universality. Nat Commun. **6**, 6664 (2015).

[22] Kaeko, K. Spatiotemporal Intermittency in Coupled Map Lattices, Prog. Theor. Physics. **74**(5), 1033-4044 (1985).

[23] Kaneko, K. Globally Coupled Chaos Violates the Law of Large Numbers but Not the Central-Limit Theorem. Phys. Rev. Lett. **65**,1391-1394 (1990).

[24] Zhou, C. & Kurths, J. Noise-Induced Phase Synchronisation and Synchronisation Transitions in Chaotic Oscillators. Phys. Rev. Lett. **88**, 230602 (2002).

[25] Pecora, L. M. & Carroll, T. L. Synchronisation in chaotic systems. Phys. Rev. Lett. **64**, 821–824 (1990).

[26] Rosenblum, M.G., Pikovsky, A.S. & Kurths, J. Phase Synchronization of Chaotic Oscillators. Phys. Rev. Lett. **76**(11), 1804-1807(1996)

[27] Klein, T., Siegwolf, R. T. W. & Körner, C. Belowground carbon trade among tall trees in a temperate forest. Science **352**(6283), 342-344 (2016)

[28] Graham, B. & Bormann, F. Natural root grafts. Bot. Rev. **32**,255–292 (1966).

[29] Lev-Yadun,S. Why should trees have natural root grafts? Tree Physiol. **31**,575–578 (2011).

[30] van der Heijden, M. G. A. et al. Mycorrhizal fungal diversity determines plant biodiversity, ecosystem variability and productivity. Nature **396**, 69–72 (1998)

[31] Simard, S. W.et al. Net transfer of carbon between ectomycorrhizal tree species in the field. Nature **388**, 579–582 (1997)

[32] Gaion, L.A. & Carvalho, R.F. Long-Distance Signaling: What Grafting has Revealed?. J. Plant Growth Regul. **37**, 694–704 (2018).

694 [33] Esmaeili,S., Hastings, A., Abbott, K., Machta, J. & Nareddy, V.R. Density
695 dependent Resource Budget Model for alternate bearing. J. Theor. Biol. **509**.110498
696 (2020)
697 [34] Ye, X. & Sakai, K. Limited and time-delayed internal resource allocation generates
698 oscillations and chaos in the dynamics of citrus crops. Chaos **23**,043124 (2013).
699 [35] Ye, X. & Sakai, K. A new modified resource budget model for nonlinear dynamics
700 in citrus production. Chaos,Solitons and Fractals.87.51-60.(2016).
701 [36] Smith, M. W. et al. Long-term performance of 'Ellendale' mandarin on seven
702 commercial rootstocks in sub-tropical Australia, Sci Hort.**102**(1), 75-89 (2004).
703 [37] Ferguson, L., Beede, R.H., Reyes, H. & Metheney, P. California Pistachio
704 rootstocks evalustaions. Acta Hortic. **591**, 63-66 (2002).
705 [38] Johnson, R.S. & Weinbaum, S.A. Variation in tree size, cropping efficiency, and
706 alternate bearing among Kerman pistachio trees. J. Am. Soc. Hortic. Sci. **112**,942–945.
707 (1987).
708 [39] Moran P.A.P. The statistical analysis of the Canadian Lynx cycle. 2.
709 Synchronisation and meteorology. Aust. J. Zool. **1**, 291–298 (1953).
710 [40] Hagerstorm, A. M., et al. Experimental observation of chimeras in coupled-map
711 lattices. Nat. Phys. **8**, 658–661 (2012).
712 [41] Sakai,K., Noguchi,Y. & Asada, S., Detecting chaos in a citrus orchard:
713 Reconstruction of nonlinear dynamics from very short ecological time series.
714 Chaos Solitons Fractals. **38**(5), 1274-1282 (2008).
715 [42] Sakai, K., Noguchi, Y. Controlling chaos (OGY) implemented on a reconstructed
716 ecological two-dimensional map. Chaos Solitons Fractals. **41**(2), 630-641(2009).

717 [43] Sugihara, G., May, R. Nonlinear forecasting as a way of distinguishing chaos from
718 measurement error in time series. Nature **344**, 734–741 (1990).
719 [44] M. Sano & Sawada.,Y. Measurement of the Lyapunov Spectrum from a Chaotic
720 Time Series. Phys. Rev. Lett. **55**, 1082 (1985).
721 [45] Packard,N. H., Crutchfield, J. P., Farmer, J. D. & Shaw, R. S. Geometry from a
722 Time Series, Phys. Rev. Lett. **45**, 712 (1980).
723 [46] Hoch,G., Siegwolf, Rolf T.W., Keel, S. G. Körner,C. & Han, Q. Fruit production in
724 three masting tree species does not rely on stored carbon reserves, Oecologia **171**, 653–
725 662 (2013).
726 [47] Tomoaki,I., Igarashi, S., Yoshida, S., Tanaka, K. , Masaki, T., Tayasu, I. Are stored
727 carbohydrates necessary for seed production in temperate deciduous trees? J. Ecol. **101**,
728 525–531 (2013).
729
730
731

Figures

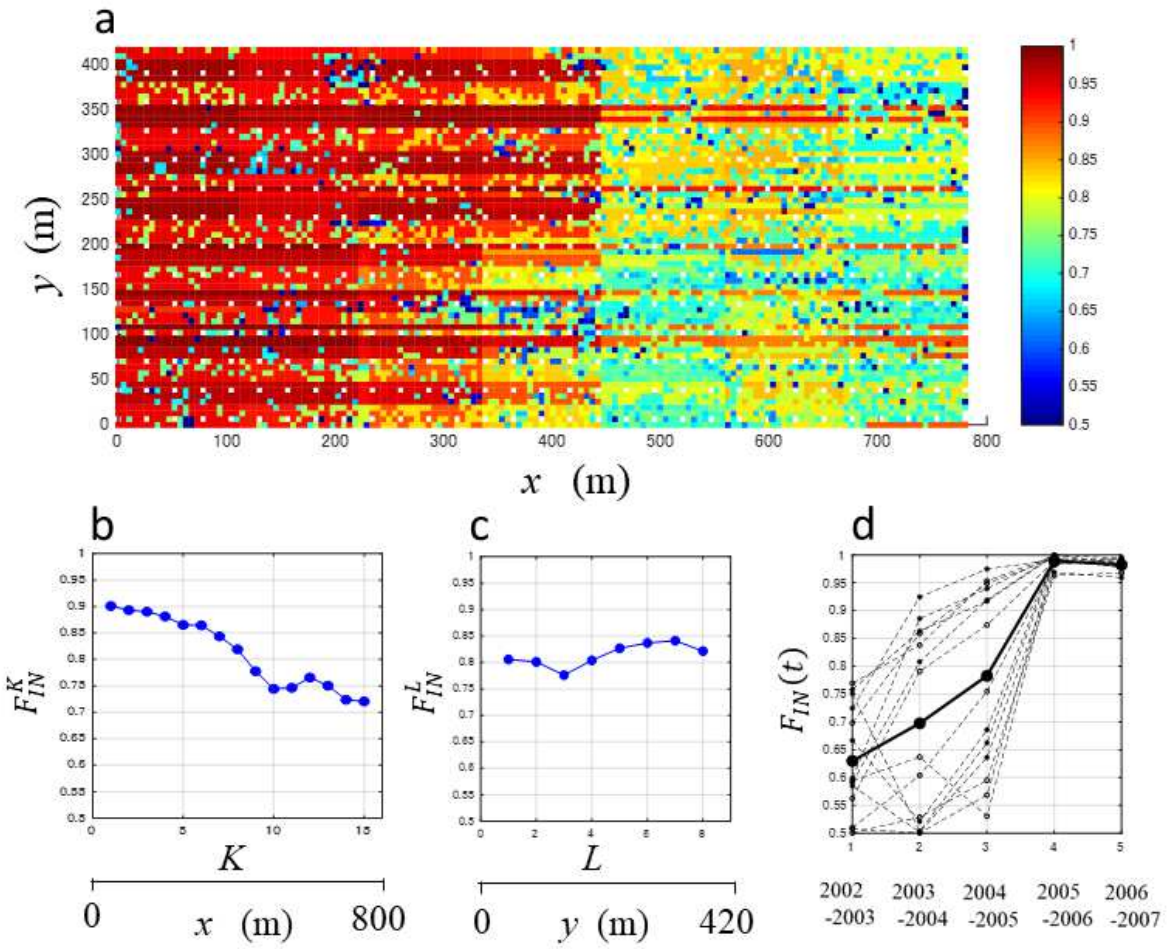

Figure 1

Spatial distributions of the in-phase synchronisation in the orchard. (a) The actual □□□ □ map for 2002–2007 in eight blocks (7 West-East × 2 South-North); (b) Averaged West-East gradient of □□□ □ for 2002–2007; (c) Averaged South-North gradient of □□□ □ for 2002–2007; (d) time (year) evolution of FIN(t).

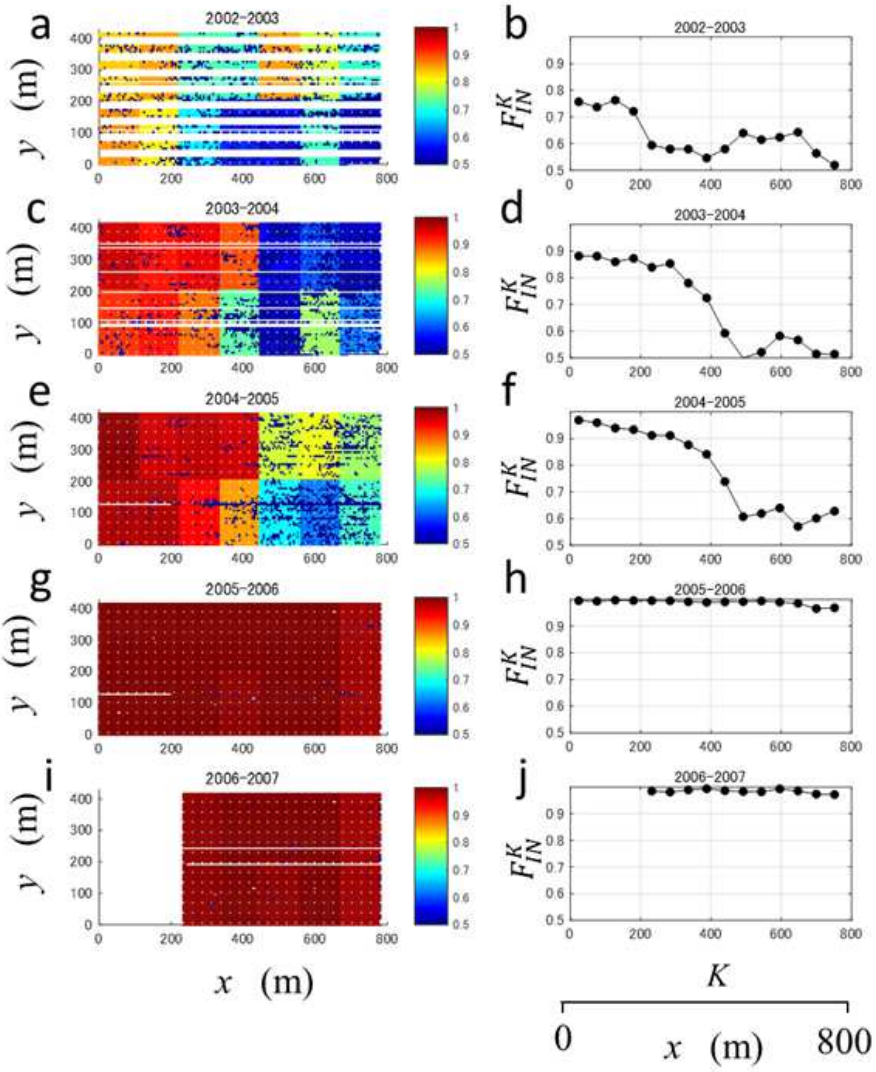

Figure 2

Time evolution of the spatial transition of the phase synchronisation (a)-(e) The time (year) changes of the spatial phase synchronisation: □□□ □ (□) maps for 2002–2003, 2003– 2004, 2004–2005, 2005–2006 , and 2006–2007 periods in the orchard (f)-(j) The gradient of the strength of the phase synchronisation: □□□ □ (□) vs. K plots for 2002–2003, 2003–2004, 2004–2005, 2005–2006 ,and 2006–2007 periods in the orchard

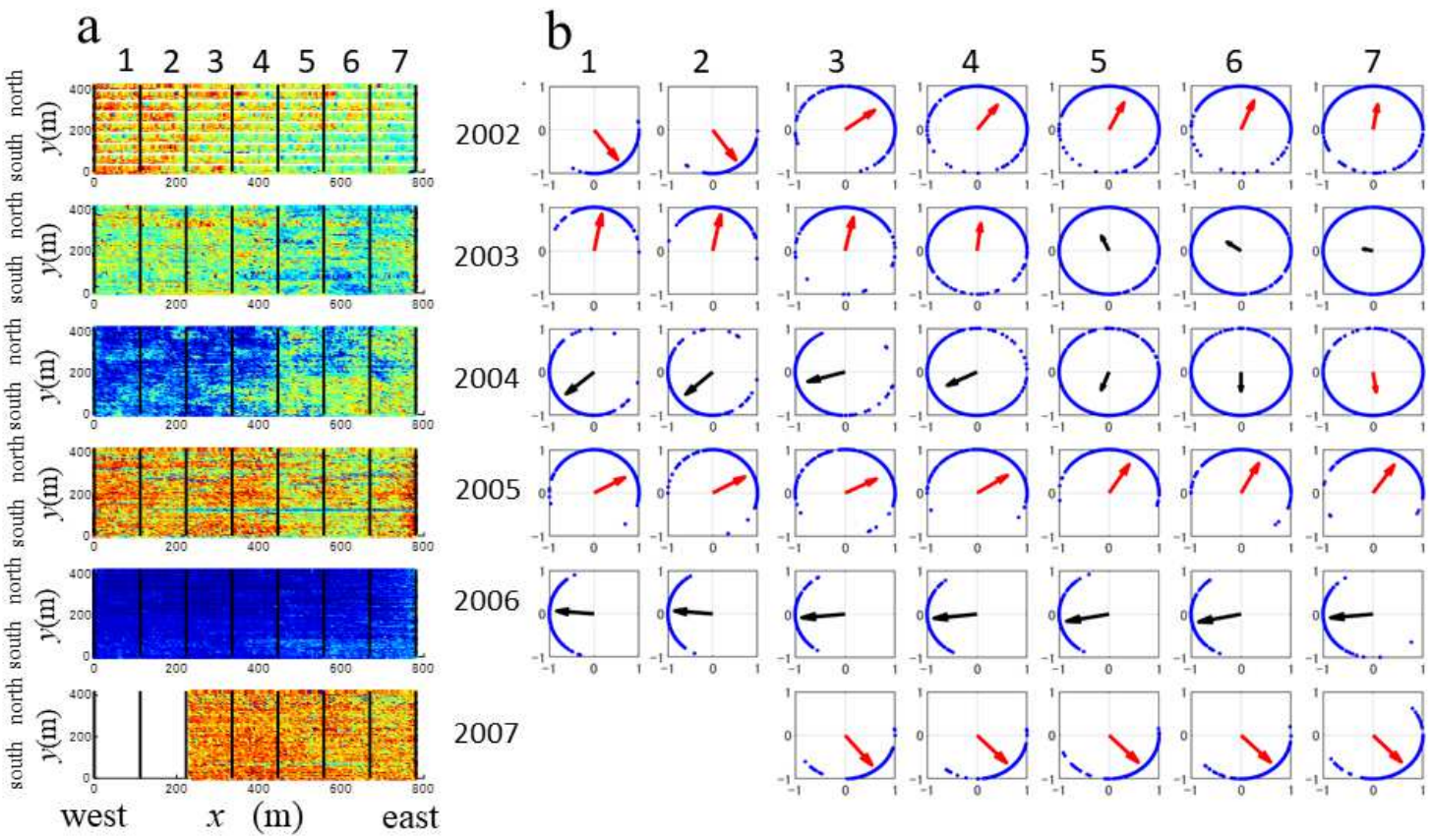

Figure 3

Spatial and annual transitions of the states of “on-year” and “off-year” for individual trees expressed by circle maps. (a) Yield maps for 2002 through to 2007. (b) Circle maps for the fourteen blocks for six years (2002–2007). The blue dot mark (cos ⍰⍰, sin ⍰⍰) on the circumference represents the state of tree i. The vectors represent the on-off state of sub-populations of each block and on and off correspond to the red and black ink, respectively.

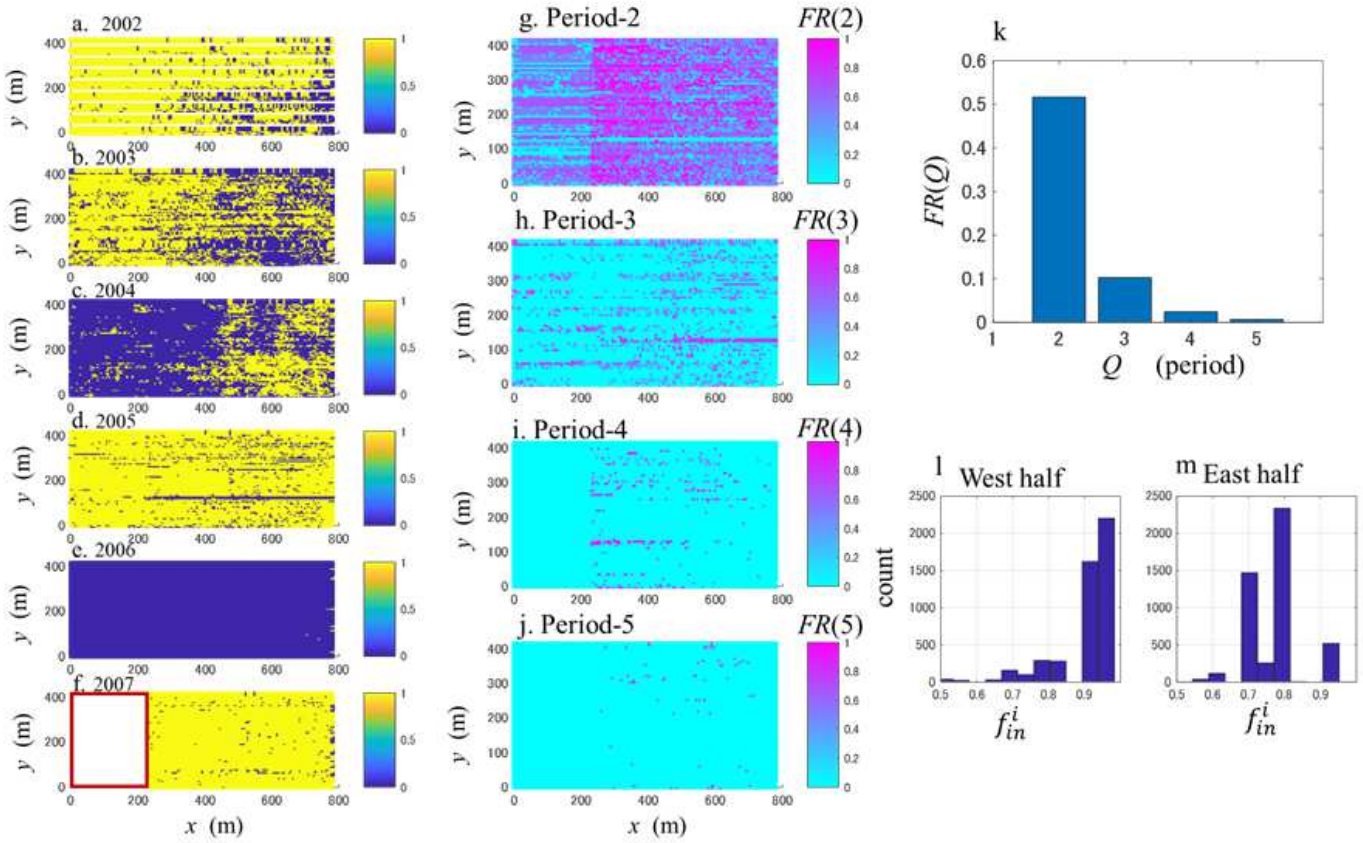

Figure 4

Spatial distribution of the periodic components for individual trees and the compositions of FR(Q) in the population. (a)-(f) On-off states of each trees for six years (g)-(j) Spatial distribution of individual fraction of period FRi(Q) for period-two (Q=2), period three(Q=3), period-four(Q=4) and period-five (Q=5), respectively. (k) The components of the periodic components FR(Q) of the population. (l) Histogram of in i in the west half of the orchard. (m) Histogram of in i in the east half of the orchard

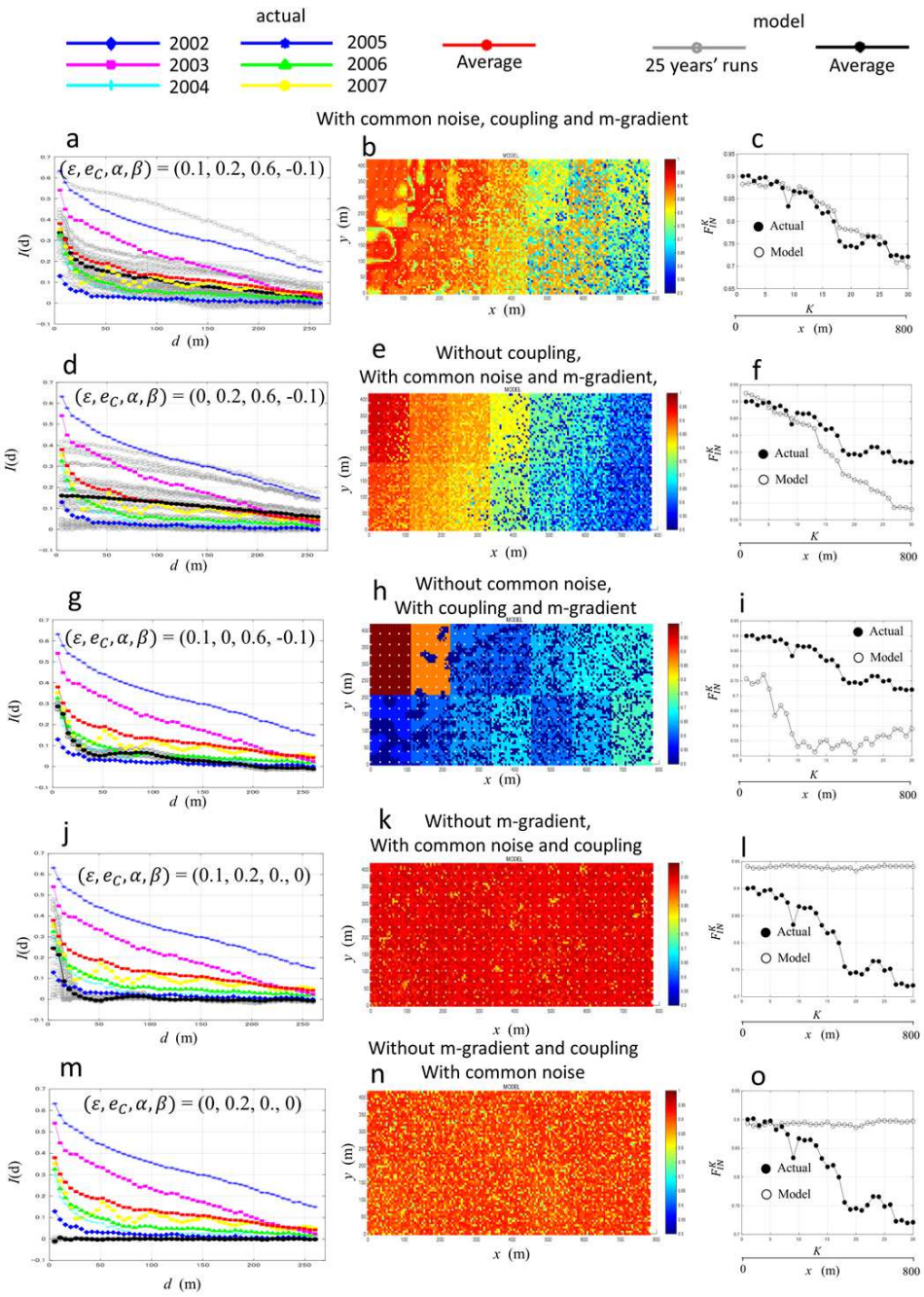

Figure 5

Demonstration of the long-ranged spatial correlations and spatial distribution of phase synchronisation realised by diffusive coupling and common noise. The parameter settings used for the numerical simulations are as follows: The first row :with the three essential factors (□, □□, □, □) = (0.1, 0.2, 0.6, -0.1), The second row : without common noise (□, □□, □, □) = (0, 0.2, 0.6, -0.1), The third row : without the local direct coupling (□, □□, □, □) = (0.1, 0, 0.6, -0.1), The fourth row : without the spatial gradient of cropping

coefficients (□, □□, □, □) = (0.1, 0.2, 0, 0) , and the fifth row : only with common noise (□, □□, □, □) = (0, 0.2, 0, 0).

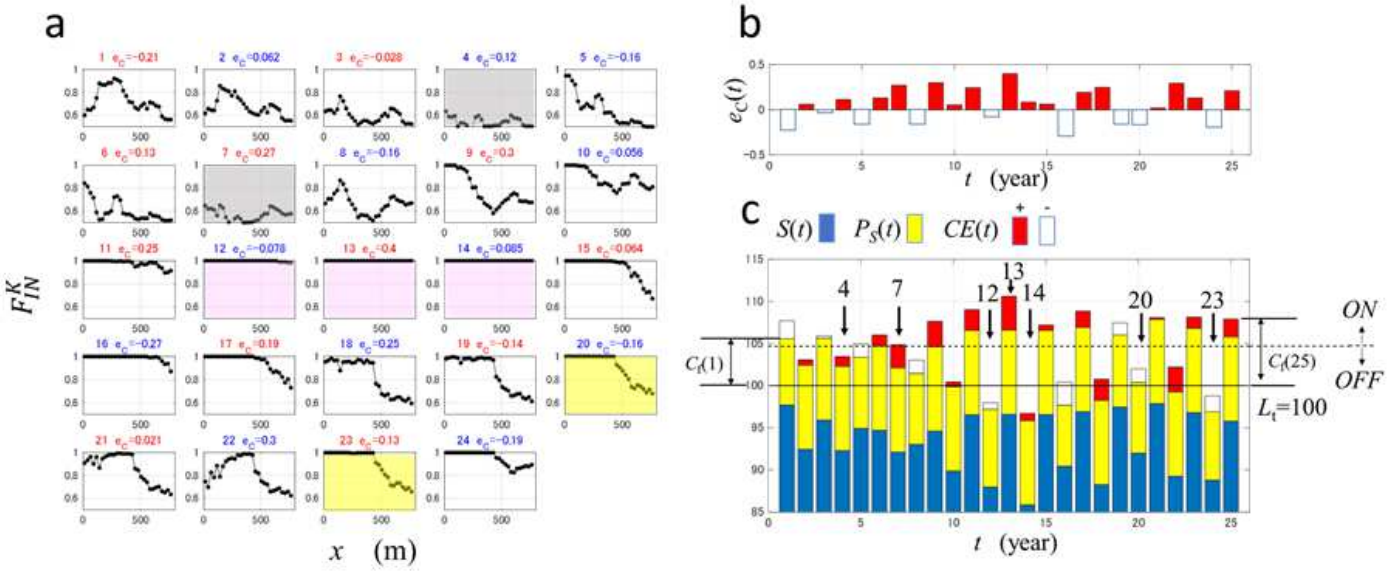

Figure 6

Spatio-temporal behaviour of phase synchronisations caused by endogenous dynamics with exogenous force. The numerical experiments were conducted with the best fit external force (common noise) eC(t) and initial values of Si(1) (i = 1, 2, …, 9,562) determined in Fig.5-(b) and calculated 24 □□□ □ (□) and FIN(t). (□, □□, □, □) = (0.1, 0.2, 0.6, −0.1) (a) 24 □□□□ (□) values are displayed for t=1,2,…24 determined from 25 years runs. (b) The time (year) history of external force (common noise) □□(□). t=1,2,…25. “red” and “white” correspond to positive and negative values of eC(t).(c) □(□) =1□∑ □□(□)□□=1, □ = 9.562 represents the total amount of resource reserves of all trees at year t. □□ (□) is the total resource added on all trees at year t. □□(□) = □0 × □□(□) is the external force (common noise) identically imposed on all trees at year t. In the bar chart, “red” and “white” correspond to positive and negative effects of external forces (common noise); CE(t), respectively. The excess of the threshold (Lt=100) of the total amount of S(t), PS(t), and CE(t) becomes the flowering cost Cf(t).

Supplementary Files

This is a list of supplementary files associated with this preprint. Click to download.

- Supplementarydataset.xlsx
- Supplementsinfo1.docx
- Supplementsinfo2.docx